A study of external heating approaches for lithium-ion pouch cells with large terminal tabs

Zhao, Rui; Chittezhath, Vinayan; MacNeil, Dean D.

Publisher's version / Version de l'éditeur:
https://doi.org/10.1016/j.applthermaleng.2026.129773
Applied Thermal Engineering, 289, 3, pp. 1-12, 2026-01-10

Applied Thermal Engineering 289 (2026) 129773

Contents lists available at ScienceDirect

Applied Thermal Engineering

journal homepage: www.elsevier.com/locate/apthermeng

Research Paper

A study of external heating approaches for lithium-ion pouch cells with large terminal tabs

Rui Zhao *, Vinayan Chittezhath, Dean D. MacNeil

Automotive and Surface Transportation Research Centre, National Research Council of Canada, Ottawa, ON K1A 0R6, Canada

ARTICLE INFO

Keywords:
Li-ion battery
Low temperature
Surface heating
Tab heating
Durability

ABSTRACT

Lithium-ion (Li-ion) batteries have significantly deteriorated energy and power performance when used at extremely low temperature, which creates difficulties when deployed in applications within cold climate. Battery preheating is critical in this aspect to improve the performance of Li-ion cells. In this work, polyimide film heaters are used to selectively preheat commercial pouch type battery cells with large terminal tabs that have been exposed to sub-zero temperatures. Two heating configurations, surface heating and tab heating, are compared in terms of their heating power, heating time, hot spot development, and temperature uniformity. Surface heating can preheat the cell from −30 °C to 0 °C in 5 min, while tab heating overheats the tabs when a high heating power is applied. Thermal modelling is then used to investigate heat transfer resistances during the tab heating configuration by adjusting the dimension of current collector and electrode tab, as well as the thermal contact resistance at the interface between the tab and current collector. Larger tabs are found to be helpful in reducing the tab temperature. However, state-of-the-art OEM cells are not equipped with such tabs that support tab heating. Finally, the durability test is performed on both the original and preheated cells, during which 10% and 22% capacity losses are found on the cells after 1000 charge/discharge cycles and 500 preheating cycles, respectively. Morphological and electrochemical analyses are conducted to investigate the fading mechanism, and it reveals that active materials and lithium ions losses lead to the degradation of performance and durability.

1. Introduction

Lithium-ion (Li-ion) batteries are the most popular battery type owing to their high energy density (up to 750 Wh L^{-1}) and long cycle life (1000–6000 cycles) [1]. They are widely used in portable devices, power tools and electric vehicles. Li-ion battery demand has quintupled from 2020 to 2024, with light duty vehicle deployments accounting for 90% of this increase [2]. The global thirst for Li-ion batteries will continue to grow in the coming decades to support the shift towards green and sustainable energy, for example a climate plan was announced in Canada to end the sales of all new light-duty vehicles powered by gasoline or diesel by 2035 [3]. Similar to other high latitude countries, cold weather is common within many large cities in Canada during the winter season.

At low temperatures, the performance and durability of Li-ion batteries are affected due to its significant reduction in the charge and discharge ability. As the charge transfer and the ion dissolution and diffusion in electrodes become difficult in cold climates, the internal resistance of Li-ion batteries increases exponentially, leading to a significant decrease in their usable power and capacity. Charging a discharged cell at low temperatures is more difficult than discharging a charged cell at low temperatures because the de-lithiated graphite and lithiated cathode have a higher charge transfer resistance at low temperatures [4], and extended use at low temperatures may lead to Li-plating [5], a serious potential safety scenario. Vikram et al. summarized the root cause of degraded performance of Li-ion batteries at low temperatures [6]. Luo et al. also reviewed the related issues and proposed potential strategies from the material perspective for improvement [7]. Inhomogeneous Li-plating due to electrode potential gradient during continuous charge and discharge cycle at 0 °C was observed by Storch et al. [8]. Laforgue et al. also noticed that the fast-charging performance of an 18,650-type cell degraded quickly when the battery temperature was below 10 °C [9]. Both the degradation in performance and safety when operating Li-ion batteries at low temperatures could be the key factors that hinders EV market penetration in countries or regions with extreme cold weather.

* Corresponding author.
E-mail address: Rui.Zhao@nrc-cnrc.gc.ca (R. Zhao).

https://doi.org/10.1016/j.applthermaleng.2026.129773
Received 22 October 2025; Received in revised form 19 December 2025; Accepted 9 January 2026
Available online 10 January 2026

To ensure that Li-ion batteries deliver optimum results at low temperatures, a preheating system within the device to warm up the batteries prior to any charge/discharge activity could be beneficial. There are two main categories of preheating approaches: internal and external heating systems [10]. Internal preheating warms up batteries internally using either the cell's own energy or external energy, while the external method transfers external thermal energy into the cell via convection or conduction from the cell wall surface. In comparison, internal heating approaches usually achieve better temperature uniformity across the cell than external heating methods due to the uniform heat generation during cells' self-heating and the reduced heat transfer distance. However, an internal approach is typically more complicated and costly to deploy, while also requiring modifications to battery cells (such as inserting additional inactive components). For example, Wang et al. designed a pouch cell with nickel foil(s) sandwiched between electrodes [11]. The inserted nickel foil acted as an internal heater and were powered by the cell's stored energy, capable of warming up the cell from −30 °C to 0 °C within 1 min. Approximately 7% of the cell's capacity was lost after 50 charge and discharge cycles (10 preheating cycles within each charge and discharge cycle). Instead of sandwiching one layer of nickel foil at the center of the cell, they used multiple nickel foils dispersed within the cell to reduce the heat transfer distance while improving the heating effectiveness and temperature uniformity [12]. In addition, alternating current (AC) can also generate heat inside cells, due to the cells' internal resistance [13]. Choosing a suitable current amplitude and frequency at different states of charge (SoCs) is critical for optimum cell heating performance. With AC heating, it is important to avoid lithium plating that occurs at high SOCs combined with high current value and low frequency since overcharge can lead to overpotential on the anodes. Zhu et al. compared heating times against applying different current amplitudes and frequencies on a 30 Ah $LiFePO_4$ cells at 50% SoC [14], and it took approximately 30 min for the system to heat the cell from −25 °C to 5 °C. Roughly 4% of the cell's capacity loss was observed on the AC-heated cells after 7 charge and discharge cycles (30 preheating cycles within each charge and discharge cycle) [15].

In contrast, external heating systems transfer thermal energy to the cell through heaters placed directly on the cell body or through a heat transfer medium. Air, liquids, or solids can be used as the heat transfer medium to carry the thermal energy to the cell, while the heat source could be waste heat from another component (heat pump, internal combustion engine), electrical space heaters or a combination thereof. For example, when we disassembled the Canadian version of the original Nissan Leaf, it used plate heaters around the battery pack to precondition the batteries at low temperatures. Many early generation EVs, e.g., Ford Escape hybrid and VW e-Golf, use air as the heat transfer medium due to its low cost and simplicity. Most recent battery electric vehicles (BEVs) and plug-in hybrid electric vehicles (PHEV), e.g., Tesla series, Ford Lightning, Polestar, etc., use coolant or refrigerant as the heat transfer medium. When plugged in and the battery temperature is below the manufacturers' pre-set value, heat will be generated through the heat pump or a positive-temperature-coefficient (PTC) heater and then transferred to individual battery cells through the liquid heat transfer medium. There is also an example of a solid composite phase change material being used to generate heat to preheat battery cells [16].

Due to the layered structure of the electrodes used in manufacturing Li-ion cells, the thermal conductivity of the cell is different in directions perpendicular and parallel to the electrodes. When cooling/heating different locations of the cell (e.g., large surface vs. edges), the rate of temperature change and temperature gradient inside the cell will be different [17]. As an example, tab cooling and surface cooling were compared within a battery thermal management system using 5 Ah pouch cells with large tables [18]. It was found that the selected cell has improved temperature uniformity and durability when cooled through the tabs compared to the surface. Subsequent research studied the trade-off between tab and surface cooling for battery cells of different sizes and tab layouts [19], as well as investigated the role of involving highly conductive ceramics to improve the cooling performance [20]. To our knowledge, no research has been performed on comparing the performance of tab and surface heating on Li-ion cells specifically for cold weather applications. In addition, literature indicates that the capacity loss of preheated Li-ion cells at low temperatures was found to be significant [15] and the side effects of multiple preheating events over the longer term on cells and their specific capacity fading mechanism are not clear. To fill this research gap, 8 Ah pouch cells with large tabs were selected for this work and either tab heating or surface heating, achieved through polyimide heaters, were compared under different applied power levels. A thermal model was also developed and used to identify the bottlenecks of tab heating and identify methods to improve the preheating process at low temperature. Finally, durability tests were performed on both a control group cell and a cell with long-term preheating cycles at a low temperature of −30 °C to investigate the changes in durability, via morphological and electrochemical analyses.

2. Experimental setup and model description

2.1. Cell selection and preparation

8 Ah NMC battery cells that have large tabs were procured online. The dimension of the tabs was 8 cm by 3 cm by 0.04 cm, while the thickness of the cell was 0.85 cm with the remaining dimension of the cell given in Fig. 1b. Prior to the preheating test, the cells were preconditioned at room temperature for 5 cycles on an Arbin battery cycler (BT-2000) with a constant current (0.5C) followed by a constant voltage (to a current value of 0.02C) charging procedure. The low temperature discharging performance of the cell was then tested in a programmable environmental chamber (Thermotron S-8-8200-MS) with temperature set to either 0 °C, −10 °C, −20 °C, −30 °C, where the cell was soaked for a full 24 h prior to performing either a 1C or a 0.5C discharge at the set temperature. All charging events were conducted at room temperature at constant current of 0.5C followed by a constant voltage with a cut-off current of 0.02C.

2.2. Preheating test

The thermocouple mounting locations during the preheating tests are shown in Fig. 1b and c. For the surface heated cell, a polyimide film heater that has an identical size as the cell was affixed to one side of the cell, where thermocouples 8, 9, and 10 were mounted on top of the heater. Thermocouple 8 was at the center and sat on the heating wire of the heater, while thermocouples 9 and 10 were on the diagonal and 1 cm from the edge of the cell and had no heating wire underneath them, as shown in Fig. 1d. For all tests, the temperature data was recorded through a data logger (Pico TC-08). For the tab heated cell, polyimide heaters that have the same size as the external cell tabs (positive and negative) were taped on one side of both tabs, where thermocouples 1 and 7 were mounted on the center of the tabs on the non-heater side. All preheating tests were performed in the environment chamber with the temperature set at −30 °C. A power supply (Agilent E3634A) was connected to the polyimide heaters, and different heating powers were delivered to the heaters. The power was turned off when the minimum temperature recorded from cell surface reached 0 °C, at which temperature the cell is safety to charge according to the specification sheet. The temperature data from all 10 thermocouples and heating time were recorded for comparison.

2.3. Durability test

The aim of the durability test was to understand the effect of multiple preheating events on the cells' durability with continuous temperature changes between −30 °C and 0 °C. During the test, two cells were used, one was cycled at room temperatures (20 °C, controlled through room

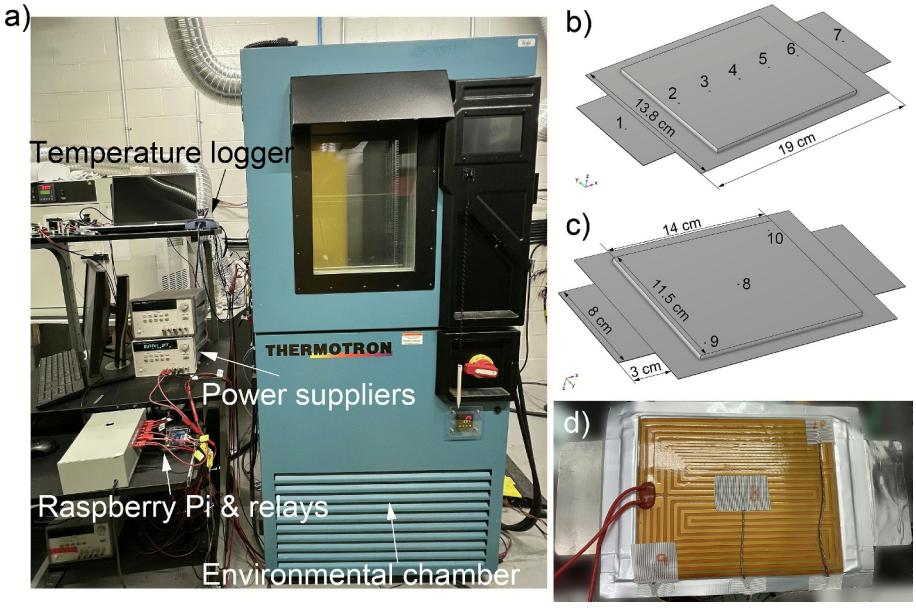

Fig. 1. a) Preheating and durability test setup; b) top and c) bottom views of the cell and the arrangement of thermocouples; and d) photograph of the surface heated cell.

HVAC system) for 1000 cycles as the control cell, while the other was cycled in the environment chamber whilst undergoing continuous surface preheating events. The environment chamber that contains the cell for preheating cycles was programmed with the following 4 steps: 1) 20 °C to −32 °C, in 10 min; 2) maintain at −32 °C for 7 h 50 min; 3) −32 °C to 20 °C, in 10 min; 4) maintain at 20 °C for 15 h 50 min (24 h in total), as shown in Fig. 2. −32 °C was programmed in the chamber during the preheating stage was to ensure that the cell can reach the set −30 °C quicker and enter the 30 min soak stage before preheating. The 1st step was to cool the environment chamber to the set temperature and have it ready for the preheating test; the 2nd step was used to conduct 5 consecutive preheating cycles (30 min soak after cell temperature dropped to −30 °C); the 3rd step would warm up the environment chamber to room temperature to be ready for a room temperature cell capacity determination (5 discharge and charge cycles and completed at a fully charged state) that was performed during the 4th step. These 4 steps were programmed into the environment chamber so that they could be repeated for 150 days.

To ensure the safety during the testing, the above tests were only conducted when a presence in the laboratory was assured, otherwise no pre-heating events occurred on the cell and the cell was held at the temperature of the environmental chamber. In addition, three thermocouples were mounted on the preheated cell, where one was on the top center of the heater, and the other two were on the opposite side center of the cell. The thermocouples at the center of the cell and on top of the heater were connected to a Raspberry Pi (a single board computer) to activate or deactivate a relay, and therefore to connect or disconnect the power supplier (25 W power output) and the heaters. The third thermocouple was used to record the cell's surface temperature through the data logger. In the Raspberry Pi program, the preheating test starts when the surface temperature of the cell drops below −30 °C for 30 min and stops when it reaches 0 °C. The preheating process was programmed to repeat 5 times. The emergency shut down function during the preheating stage would be initiated if the heater's temperature reaches 70 °C. The 5 charge and discharge cycles during step 4 were conducted through the Arbin cycler, where the charging and discharging rate was set to 1C with a cut-off current of 0.02C during the constant voltage charging stage. There was a 10-min rest between charge and discharge (same for the control group cell).

To investigate the failure mechanism of the cell that underwent the continuous preheating cycles, the incremental capacity of the cells and the surface morphology of the electrodes were analyzed through inspecting their dQ/dV curves and SEM images. Both cells were fully discharged to 3 V at 0.1C before disassembling them inside a fume hood. Samples of the anode and cathode were taken from the top, center, and bottom sections of the cell to investigate the effect of the generated temperature gradient from the heaters on their morphology, and their thicknesses were measured using a micrometer. All samples for surface morphology analyses were cleaned in a dimethyl carbonate (DMC) solution prior to the SEM analysis (Hitachi SU5000 FE-SEM).

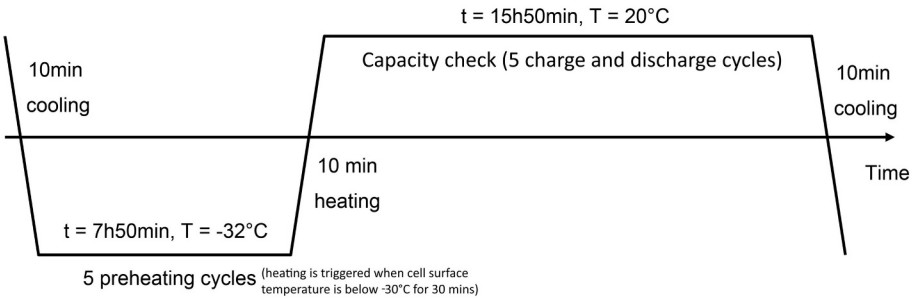

Fig. 2. One-day temperature schedule of the environment chamber during the durability test (for illustration only and not to actual scale).

2.4. Thermal model description

A 2D thermal model was developed using the COMSOL Multiphysics finite element solver to facilitate the understanding of the thermal gradients developed and heat transfer limitation during the tab preheating process. Fig. 3 shows four different geometries investigated within the thermal models, in which the electrodes, current collectors, separators inside the electrochemical cells were simplified by introducing multiple thicker current collector layers and active materials layers. The purpose of comparing the geometries with different numbers of current collector/active material layers is to ensure the model is accurate while efficient in computing as more detailed geometry would need a higher computational cost. Fig. 3a shows the geometry of the single-layer model (1 layer of copper current collector and 1 layer of aluminum current collector), where the positive tab is on the left and the negative tab is on the right side of the cell, and they are next to each other and placed in the center of the cell (marked as blue). The grey rectangles on the top and bottom of the current collectors are the active materials section. In the single-layer model, the adjusted thickness of the positive/negative current collector is the sum of all positive/negative current collectors. For multi-layer models, the adjusted thickness of current collectors equals to the total thickness of current collectors divided by the number of current collectors used in the models. A total of 37 layers of aluminum current collectors and 38 layers of copper current collectors were found inside the disassembled cell used in this study. The detailed dimensions and properties of the components of the electrochemical cell are provided in Table 1.

The cell temperature can be estimated from the thermal model by calculating the energy balance equation within the finite element meshes [21]:

$$\rho c_p \frac{dT}{dt} = \nabla \bullet (k\nabla T) + q \tag{1}$$

where ρc_p is the volumetric heat capacity of the cell, T is the temperature, t is the time, k is the thermal conductivity, and q is the volumetric heat generation term, i.e., the heat output from the polyimide heaters. Due to the thin structure of the polyimide heaters, they are physically neglected from the model except for their power output. The thermal properties of the adjusted current collectors and tabs are taken from Table 1, while the active material layers and their volumetric heat capacity is calculated as follows:

$$\rho C_p = \sum_i \frac{\rho_i C_{p,i} l_i}{l} \tag{2}$$

where i represents the components inside the electrochemical cell except the current collectors, and their thermal conductivity in x and y directions are calculated as:

$$k_x = \sum_i \frac{l_i}{l} k_i \tag{3}$$

$$k_y = \frac{\sum_i l_i}{\sum_i \frac{l_i}{k_i}} \tag{4}$$

In the model, both tabs are in direct contact with the single layer current collectors (represented by a pile of current collectors) on both sides of the cell. A closer view of the tab-current collector interface is given in Fig. 3b. In the thermal model, the thermal resistance at the

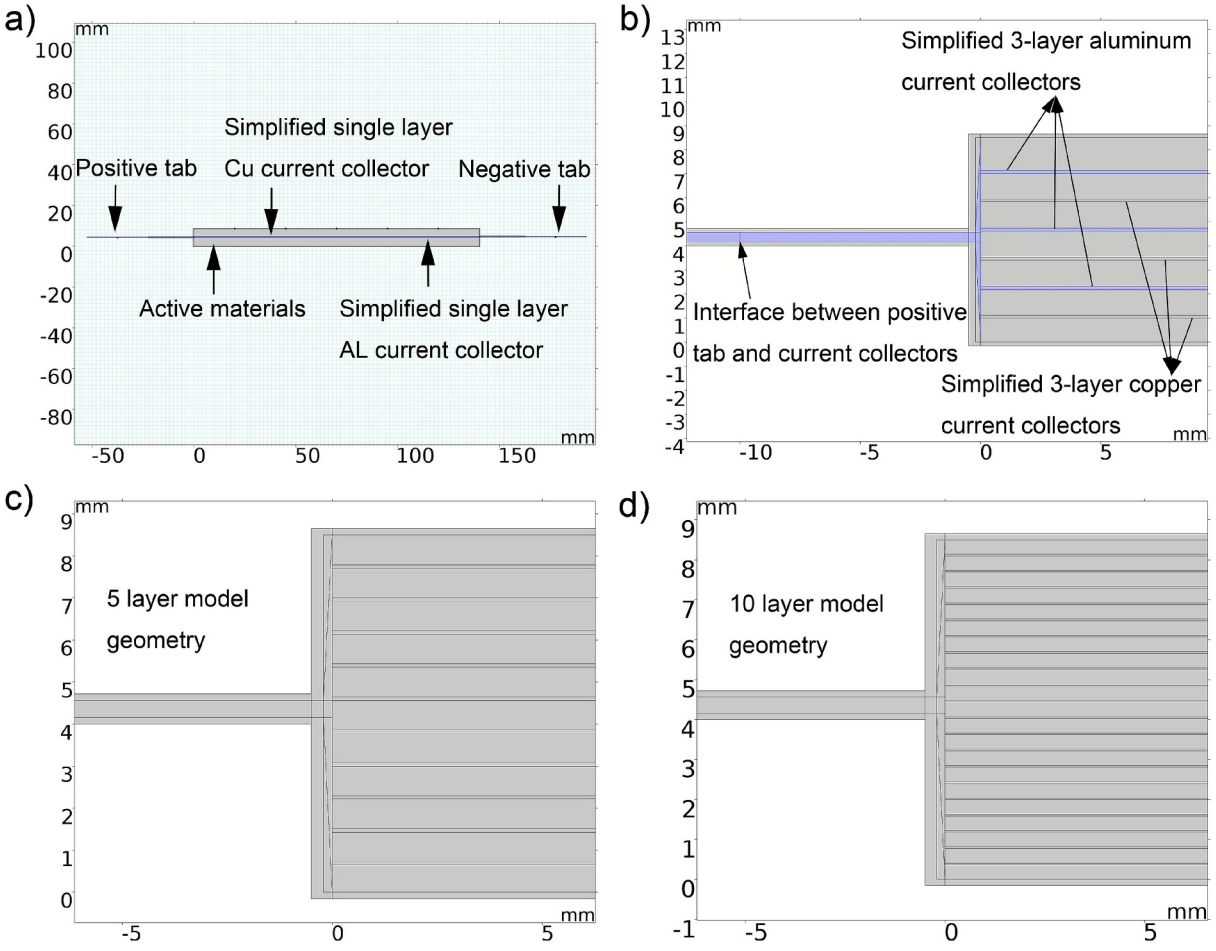

Fig. 3. Geometries describing the a) single-layer, b) 3-layer, c) 5-layer, and d) 10-layer thermal model.

Table 1
Dimension and thermal properties of the cell used in the thermal model.

Parameter	Negative tab	Cu foil	Anode	Separator	Cathode	Al foil	Positive tab
l_i (μm)	400	9	37.5	35	24	12	400
k (W m^{-1} K^{-1})	398	398	5	0.334	5	238	238
ρ (kg m^{-3})	8930	8930	2500	1009	1500	2702	2702
C_p (J kg^{-1} K^{-1})	385	385	700	1978	700	903	903

interfaces needs to be considered,

$$R_c = \frac{\Delta T}{\dot{q}} \tag{5}$$

where R_c is the thermal contact resistance, while ΔT and $\dot{q}$ are the temperature difference and heat flux across an interface, respectively. At a solid-to-solid contact interface, the joint thermal contact resistance can be expressed as:

$$R_c = \frac{1}{h_j A} \tag{6}$$

where h_j is the joint heat transfer coefficient and A is the contact area. In this work, an equivalent thin resistive layer model was used. A trial-and-error methodology was used to obtain the thermal contact resistance that provided the best match between the simulation and experimental results.

A convection heat transfer boundary condition is applied to the edges of the cell, and the heat flux across the boundary remains the same and can be expressed as:

$$-k\frac{\partial T}{\partial n} = h(T - T_{amb}) \tag{7}$$

where h is the convection heat transfer coefficient and the subscript *amb* indicates the ambient condition. For all preheating tests, 3 cm thick polystyrene insulation boards (Isolofoam HD 160) were cut into the same size as the cell surface and tab, and placed on both sides of the cell to ensure a minimal heat loss to the environment and avoid the noise from the temperature fluctuation of the environment chamber. An equivalent convection heat transfer coefficient was used in the thermal model instead of having insulation layers. The equivalent convection heat transfer coefficient was obtained by heating a reference aluminum plate with the same insulation boards wrapped and matching its cooling profile with simulation, and a value of 1.8 W m^{-2} K^{-1} was found to provide the best match and used in this work.

3. Results and discussion

3.1. Preheating tests

The discharge curves of the cell at different temperatures are plotted in Fig. 4. The performance of the cell degrades significantly with a decrease in operating temperature. At 20 °C the cell can deliver a capacity of 8.16 Ah at a 1C discharge rate, and it drops to 5.68 Ah and 3.76 Ah at 0 °C and − 10 °C, respectively. As temperature dropped to −20 °C and − 30 °C, the voltage of the cell fell quickly below 3 V (the cut-off voltage during discharge) at 1C discharge rate with no energy delivered. After reducing the discharge rate of the cell to 0.5C, the cell was able to discharge and a capacity of 1.96 Ah at −20 °C, but the cell was unable to deliver any noticeable capacity at −30 °C even when the rate of discharge rate was reduced to 0.1C. The deterioration in low temperature performance is due to the significantly increased internal resistance within the cell.

Fig. 5 shows two examples of the preheating curves of the cells using either a 63 W surface heating or a 36 W tab heating. These two chosen power outputs are the maximum outputs that were used in this work for each heating method. The heating curves (as measured on the cell) are

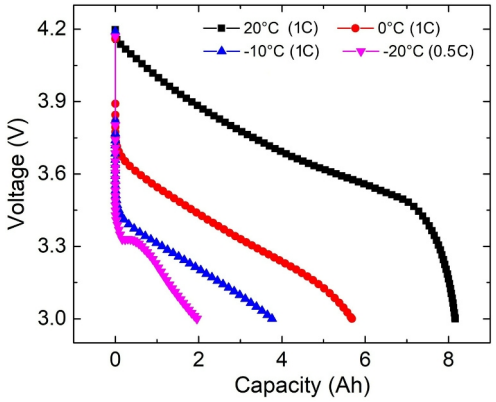

Fig. 4. Discharge profiles of the cell at different temperatures, where the discharge at −20 °C was conducted at 0.5C and the discharge rate was 1C for the other temperatures.

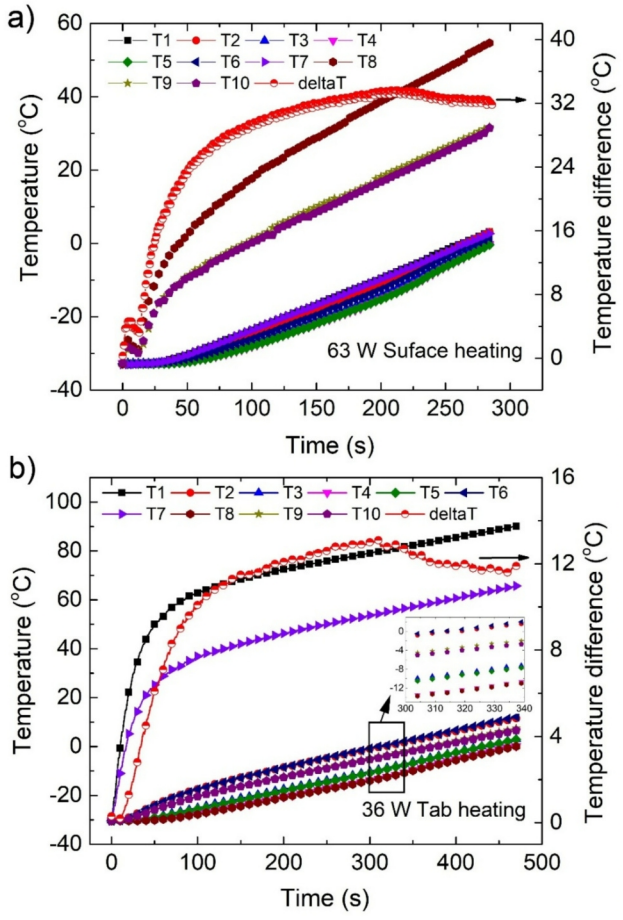

Fig. 5. Heating curves of the cells during a) surface and b) tab preheating tests at −30 °C.

nearly linear during the entire heating process for both tests and a shorter preheating time was observed during the surface heating due to the higher power output. It took less than 5 min to warm up the cell from −30 °C to 0 °C during the surface preheating test, while it took about 8 min for the tab preheating test. Higher temperatures are recorded from thermocouples placed closer to the heaters, as expected. For the surface heating test, the temperature at T_8 is much higher than the temperature of T_9 and T_{10}, which is because thermocouple #8 was placed directly on top of the heating wire to observe the heater's temperature. For the tab heating test, the temperature of the positive and negative tabs reaches 90 °C and 66 °C by the end of the test, respectively. The relatively higher temperature on the positive aluminum tab is attributed to its lower volumetric heat capacity and thermal conductivity of aluminum. Besides temperature, the maximum temperature difference of the recorded locations (excluding the temperature of tabs and T_8 during the surface heating) is also plotted over time. This is a reflection of the temperature uniformity of the cell during the preheating process. The maximum temperature differences are roughly 32 and 13 °C during the surface and tab heating tests, respectively. The higher temperature gradient across the cell during the surface heating is due to the higher heating power and thermal resistance in the heat transfer path, which will be further explained in the follow section. A more detailed analysis of the temperature data during the tab heating test is provided in the inset of Fig. 5b. It is seen that T_2 and T_6, T_3 and T_5, T_4 and T_8, as well as T_9 and T_{10} are overlapped with each other, indicating the temperature is symmetrically distributed along the cell.

In Fig. 6a, a summary of heating time for both surface and tab preheating is plotted against applied heating power, where each dot represent a preheating test with its heating power and time to warm up the cell from −30 °C to 0 °C. The heating time of both tests show an exponentially decaying pattern. The exponential fit of the surface heating data is plotted in Fig. 6a to show this pattern. The fit agrees with the surface heating data with an adjusted R-square of 98.98%. Meanwhile, the tab heating results also have a good agreement with this exponential fit when the heating power is low (≤ 22.5 W), which indicates that at a given low heating power, the heating effectiveness of both heating methods is similar. Some deviation is observed as the heating power increases, which is mainly attributed to the higher heat loss due to the overheated tabs. Fig. 6b shows the maximum temperature recorded on the surface of the cell and the tabs. Clearly, the surface heating setup can withstand a higher applied heating power than the tab heating. The tabs can easily get overheated when heated at a high applied heating power due to the small heat capacity of the tabs and the inefficient heat transfer between the tabs and cell. As temperature reaches 70 °C, there is a transition from cohesive to adhesive failure within the adhesive tape used within the heater [22], thus, the temperature of the tabs needs to be controlled below 70 °C so that the heaters will not fell off from the tabs during the preheating process. In Fig. 6b, it is seen that the tab can reach 70 °C when the heating power is higher than 27.2 W for tab heating, and the corresponding heating time is 10 mins. In other words, with the current configuration, it will take at least 10 mins for the cell to warm up from −30 °C to 0 °C through the tab heating approach. As for the surface preheating, the cell can be warm up from −30 °C to 0 °C within 5 min when the heating power reaches 56 W, and there is still room to further reduce the preheating time through increasing the applied heating power.

In contrast to the efficient cooling performance of the tabs described in the literature [18], the compromised preheating performance, as illustrated in this work, is due to the different requirements between preheating and cooling. For preheating, the battery needs to reach the set point as quickly as possible and the required energy is related to the heat capacity of the cell, while for cooling, the process is not time-sensitive and the cooling rate required is related to the heat generation rate from the battery, which varies between cells. In addition, during cooling, the low temperature on the tabs usually does not pose a safety risk to the cell, but this will be an issue during preheating due to

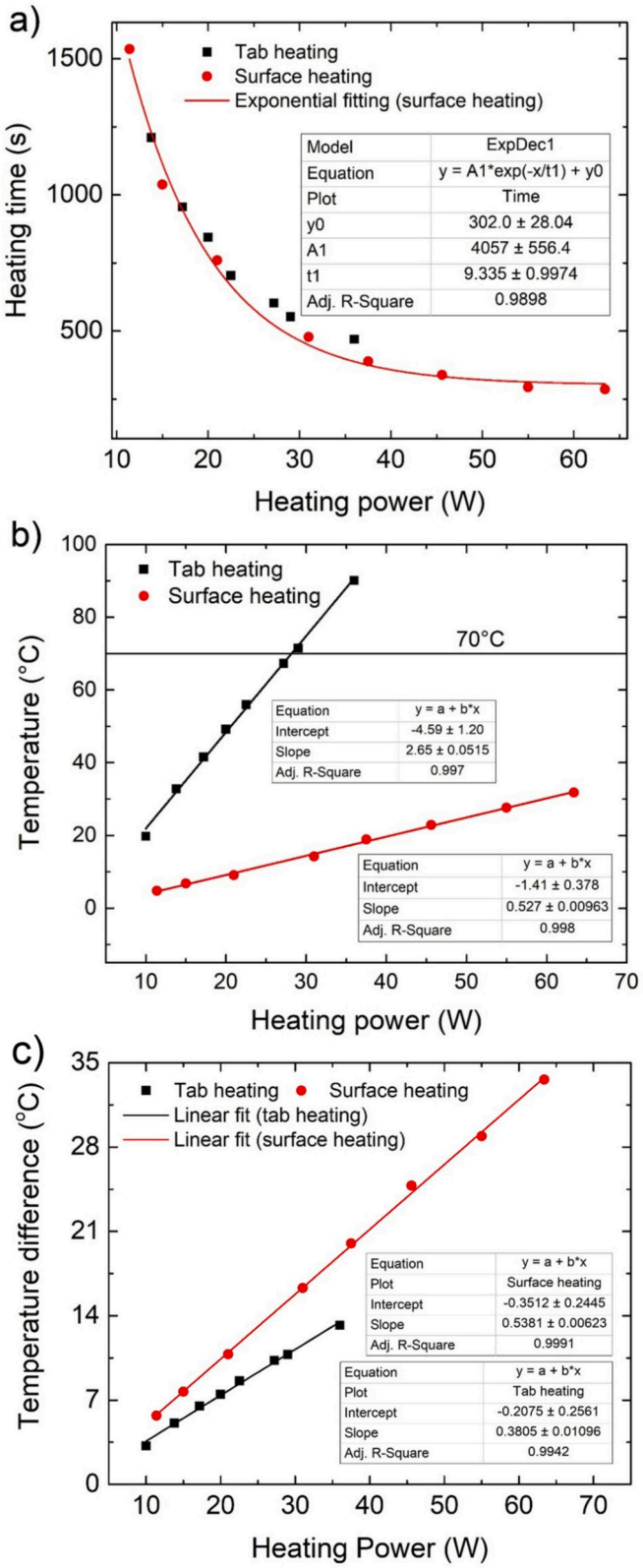

Fig. 6. Summary of the a) heating times, b) maximum tab/cell temperature, and c) maximum recorded temperature difference on the cells during the tab and surface preheating tests. All preheating tests were performed at −30 °C.

overheating.

Besides the heating time, the temperature uniformity during the preheating test was also studied. Fig. 6c summarizes the maximum recorded temperature difference (excluding the tab temperature and heater temperature) of the cells at different heating powers. It is seen that for both heating approaches, the maximum temperature difference shows a linear relationship with heating power. In comparison, the slope of the linear fit of the tab heating approach is less than that of the surface heating approach, indicating a better temperature uniformity across the cell when using the tab heating approach.

The temperature distribution along the heat transfer path can be explained through the concept of thermal resistance:

$$\Delta T = R \times \dot{q} \tag{8}$$

where R is the total thermal resistance in the heat transfer path and $\dot{q}$ is the heat flux. The thermal resistance consists of contact thermal resistance and bulk thermal resistance. To simplify the explanation, only the bulk thermal resistance of the cell in the direction of heat transfer is considered.

$$R = \frac{l}{k} \tag{9}$$

where l is the length of the heat transfer path and k is the thermal conductivity in the direction of heat transfer. For surface preheating, the heat transfer length is the thickness of the cell and k is the thermal conductivity in the thickness direction, while for tab preheating with tabs on both sides of the cell, the heat transfer length is half the length of the cell and k is the thermal conductivity in length direction. The surface heating can have a better temperature uniformity if heaters are used on both sides of the cell, which will shorten the heat transfer length by half. Similarly, if the tabs are only designed on one side of the cell, the temperature difference across the cell preheated through tabs is about to be doubled.

3.2. Thermal modelling of the tab heating

In this section, a 2D thermal model described in Section 2.4 was used to understand the heat transfer process of the tab preheating approach and its bottleneck. The effects of multiple parameters, including thickness of current collectors, tab dimension, and interface thermal contact resistance, on the preheating performance is modelled and discussed. In addition, pouch cells that were disassembled from commercial EVs are compared with the cell used in this work in terms of their dimensions and tab sizes to better understand if the tab heating approach can be used for the current EV pouch cells.

Fig. 7a shows the simulated T_1 (aluminum tab (+) during preheating, hot spot) and T_4 (cell center temperature, cold spot) calculated using the single-layer, 3-layer, 5-layer, and 10-layer models given in Fig. 3. The simulated temperature profiles from these four models are overlapping with each other except for a slight offset (~1 °C lower) from the single-layer model, as shown in the inset. The number of the domain elements in the mesh of these models are about 3×10^4, 9.5×10^4, 2.5×10^5, and 9.2×10^5 respectively. To ensure the accuracy and efficiency of the model, the 5-layer model was used for the following simulations. A trial-and-error method was used to find the equivalent thermal contact resistance between the tabs and current collectors, and the obtained value is 10^{-5} K m^2 W^{-1}. Fig. 7b to d compare the measured and simulated temperature profiles from locations 1, 2, 4, and 7 shown in Fig. 1b at different preheating powers. The model provides a good prediction of the entire preheating process for a wide range of preheating power and time. The model also validated that the higher temperature on the aluminum positive tab was due to the material that the positive tab used.

To understand the bottleneck towards heat transfer for the tab heating process, four parameters: 1) thickness of current collectors, 2) thermal contact resistance between tabs and current collectors, 3) tab width, and 4) tab thickness, were varied to investigate their effects during preheating using 36 W as applied power. In Fig. 8a, T_1 and T_4 of the cells are plotted using the original and thicker current collectors, where c1 indicates the original combination of 9 μm copper and 12 μm

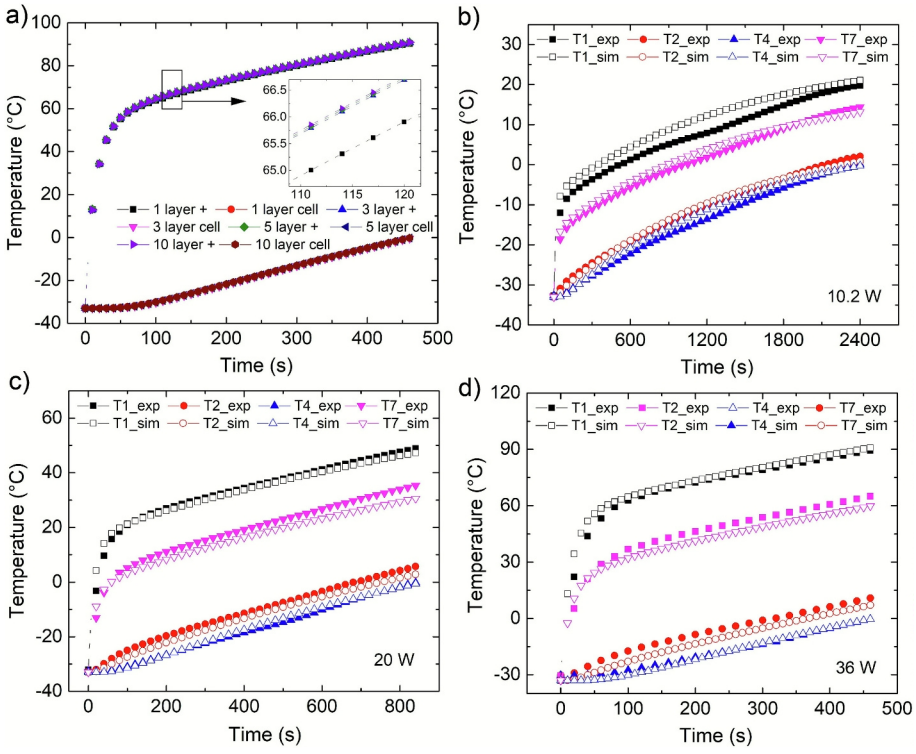

Fig. 7. a) Comparison of the simulation results using the single-layer, 3-layer, 5-layer, and 10-layer geometries; Comparison between the simulation and experimental results of the b) 10.2 W, c) 20 W, and d) 36 W tab preheating tests on a 5-layer thermal model.

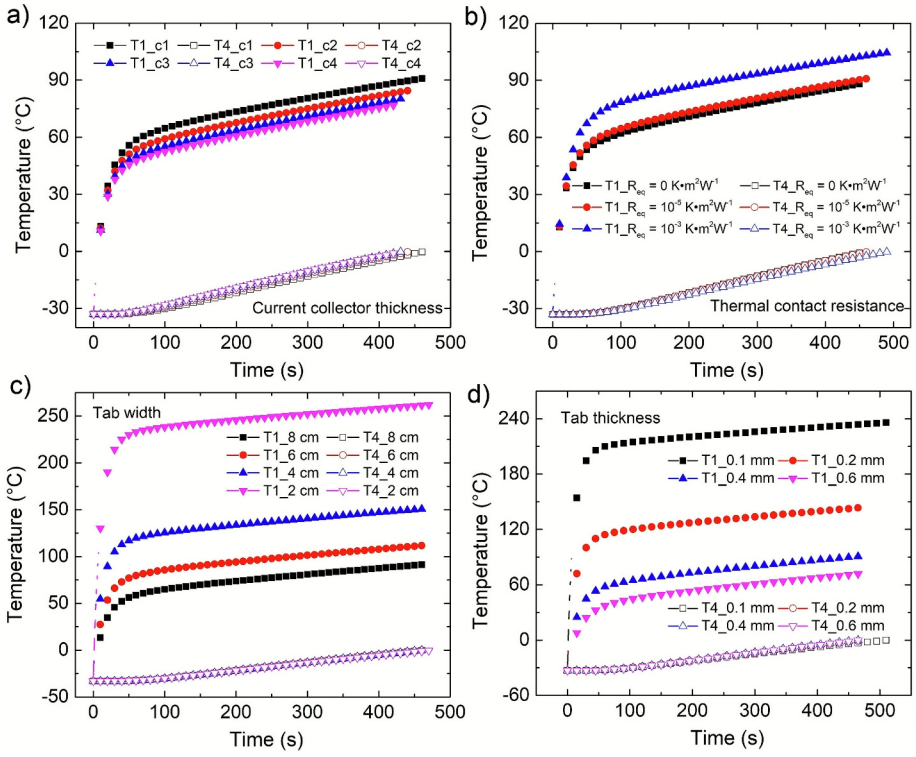

Fig. 8. The effects of a) current collector thickness, b) thermal contact resistance, c) tab size, and d) tab thickness on the tab preheating performance.

aluminum current collectors, while c2, c3, and c4 indicate the combinations of 12 μm and 16 μm, 15 μm and 20 μm, and 18 μm and 24 μm copper and aluminum current collectors, respectively. With using thicker current collectors, there is a slight improvement on the preheating efficiency and overheated tabs, however, the improvement is not sufficient to compensate for the increased cost and reduced energy density of the cell. Fig. 8b shows the temperature profiles of the cell using different thermal contact resistances at the joints between tabs and current collectors. The red circles indicate the original condition, while the black squares and blue triangles indicate the perfect thermal contact condition and a worse scenario with 100 times higher thermal contact resistance, respectively. It is seen that the thermal contact between tabs and current collectors in the original cell is close to the perfect condition, therefore, it is not the bottleneck that limits the heat transfer between the tabs and cell.

Before stepping into the discussion of Fig. 8c and d, several commercial EV battery packs were obtained and five different EV pouch cells (Fig. 9) were compared for a number of dimensions identified in Table 2. Compared to the cell tested previously, the EV cells are larger but with smaller tabs. The tab area of the test cell is more than twice that of the EV pouch cells and its tab is thicker than most of the EV cells. To investigate the effects of tab size and thickness on the preheating performance, simulations were performed on the test cell with different tab widths and thicknesses. In Fig. 8c, a sweep simulation was performed by reducing the width of the tabs of the original cell from 8 cm to 6 cm, 4 cm, and 2 cm, where the tab temperature increases significantly as the tab becomes narrower, which is attributed to the reduced heat capacity of the tabs and increased thermal resistance between the tabs and cell. Similar results are also observed when the thickness of the tabs decreases, as shown in Fig. 8d. When reviewing the tab geometries of the EV pouch cells, it can be concluded that they are not suitable for the tab heating approach since the tabs were designed mainly considering the maximum operating current for the cell, and they are not large or thick enough to effectively transfer thermal energy to the body of the cell without rapidly overheating. In addition, the heat transfer distance from the tab to the far edge of the cell (if tabs are on one side of the cell) or to the centerline of the cell (if tabs are on both sides of the cell) is longer in the EV cells than the test cell, which will lead to an uneven temperature distribution along the heat transfer path. In order to implement tab heating on the obtained EV pouch cells, the cells need to be redesigned to consider heat transfer distance, and the tabs themselves need to reduce their thermal resistance and increase their heat capacity through design improvements or material choice.

Moreover, when taking a closer look at the welding spots on the tabs of some EV cells, for example those seen in the middle and bottom rows of Fig. 9, they are not smooth nor flat and would be difficult to properly mount adhesive heaters. A compromised contact between the tab and the adhesive heater, as well as any vibration during driving, would lead to significantly higher thermal contact resistance between the heaters and tabs, which will lead to overheated heaters. In contrast, a surface preheating approach would be more feasible for these EV cells as the heaters are sandwiched between cells, which make the installation process easier and the preheating system more reliable. As can be seen in the top right corner of Fig. 9, one of the modules has thin aluminum plates sandwiched between cells to achieve the role of thermal management.

3.3. *Durability test and failure analysis*

To investigate the long-term effect of exterior heating from a low temperature on a cell's performance and lifespan, durability tests were conducted on the cells cycled in ambient condition (the control group) and cycled following the preheating cycle procedure described in Section 2.3. Fig. 10a shows the cells' capacity over the entire durability test and their linear fit (only used to roughly estimate the degradation slope). It can be seen that the cell cycled in ambient conditions (black squares) has better capacity retention than the preheated cell. The control cell retains a capacity of 7.4 Ah after 1000 cycles, which is about 90% of the initial rated capacity. While the preheated cell had a capacity loss rate more than 3 times higher that of the control cell as determined by the slope of the linear fits, having only retained a capacity of 6.25 Ah after 500 preheating cycles, which is less than 80% of the rated capacity.

Fig. 9. A photograph of OEM pouch cells and modules used in EVs.

Table 2
Dimensions of some OEM pouch cells.

	Length (cm)	Width (cm)	Thickness (mm)	Cell area (cm^2)	Tab length (cm)	Tab width (cm)	Tab thickness (mm)	Tab area (cm^2)
Test cell	14	11.5	8.8	161	80	30	0.4	24
Cell 1	19	14.5	5.4	275.5	45	20	0.13	9
Cell 2	30.5	13.5	12.5	411.8	105	5	0.45	5.25
Cell 3	24.5	11.2	11.5	274.4	45	6.4	0.36	2.88
Cell 4	20	10	11.4	200	45	11	0.12	4.95
Cell 5	23.5	14	5.9	329	100	5.3	0.23	5.3

In Fig. 10b and d, the charge and discharge curves of these cells at selected cycle numbers are plotted. It is clear that the discharge voltage plateaus of the cell cycled at ambient temperature (Fig. 10b) are higher than that of the preheated cell (Fig. 10d), while the charge voltage plateaus are lower. This is attributed to the lower internal resistance and overpotential of the control group cell. Meanwhile, with more cycles added to the cells, it can be seen that the capacity of both cells drops and the voltage plateau becomes lower for discharges and higher for charges. Alternatively, the change in the voltage plateau of the control cell is substantially smaller than that of the preheated cells, indicating a small increase of the cell resistance and good retention of the power over time, while the significantly increased overpotential of the preheated cell indicates more energy, power, and capacity losses over time. This degradation is especially obvious during the constant current charges, and it is seen that after 500 cycles, the constant current charge time of the cell is about half of that during the first cycle.

The incremental capacity plots are usually used to analyze the capacity fading of electrochemical cells [23,24]. The plots of both cells during charge and discharge at selected cycles are also plotted in Fig. 10c and e. It is seen that the intensity of the peak decreases slightly

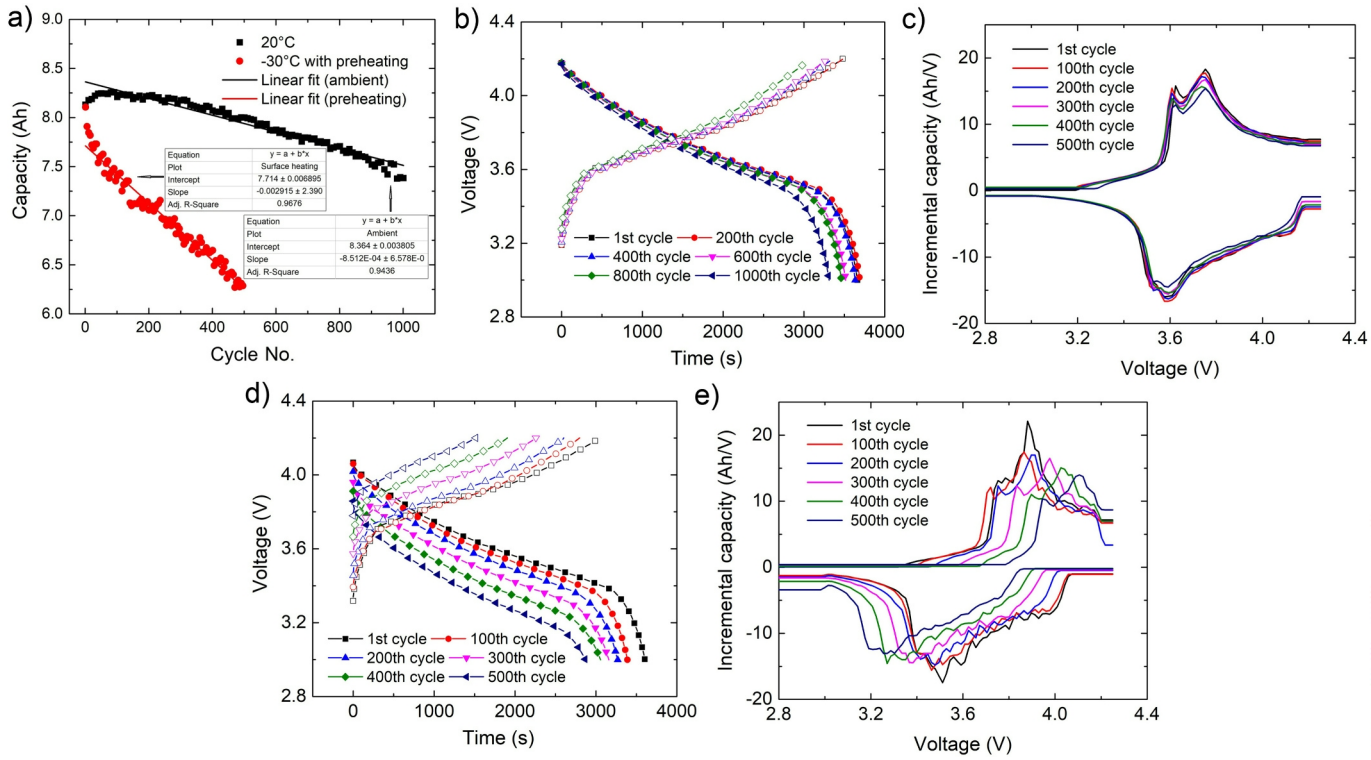

Fig. 10. Durability test results summary: a) Capacity data of the cells cycled in ambient and cycled with preheating; voltage profiles of the b) control group cell and d) preheated cell at selected cycles; and incremental capacity plots of the c) control group cell and e) preheated cell at selected cycles.

with cycle number for both charges and discharges of the control cell, indicating its capacity loss [25], and its internal resistance is relatively stable as there is no obvious shift of the peaks [26]. For the preheated cell, both peak shifts and peak intensity drops are observed. This further reveals that the performance and durability degradation of the control group cell is mainly due to capacity loss, while its from both capacity loss and internal resistance rise for the preheated cell.

To explain the difference between the failure modes of these two cells, they were disassembled inside a fume hood and samples of the positive and negative electrodes were taken from the top, center, and bottom sections of the cell. The thicknesses of the electrodes were measured at 10 different locations. The average negative electrode (2 layers of anode and 1 layer of copper current collector) thickness of the control group cell was 85.3 μm with a standard deviation of 0.68 μm, which is 4.7 μm (5.2%) thinner than the preheated cell (average thickness of 90 μm with a standard deviation of 1.56 μm). As for the positive electrodes, both cells have a similar thickness (~61 μm). Meanwhile, no differences in thickness and appearance were found between the electrodes taken from different sections of the cells.

The electrode samples were then cleaned using a solution of DMC prior to analysis within an SEM. Fig. 11a-f show the SEM images of the anodes from both cells. Specifically, the SEM images of the anodes from the top, center, and bottom sections of the preheated cell are given in Fig. 11a, b, and c, respectively. Fig. 11d and e are the images of the anodes from the top and center sections of the control group cell. Fig. 11f is the zoomed image of the red square area shown in Fig. 11b. After comparison, it is clear that the cell that underwent preheating had a rougher anode surface than the cell cycled in ambient conditions. This is mainly due to the well-known exfoliation of the graphite layers, as can be seen in Fig. 11f. With continuous temperature changes between −30 °C and 0 °C, the electrolyte that penetrated through the graphite can freeze and melt, which can cause the expansion of the graphite. Once the fresh graphite layers are exposed to the electrolyte, it will consume lithium ions and form new solid electrolyte interface, which lead to the loss of active materials and lithium ions, and resistance increase [27]. This also explains the thicker negative electrodes that was found in the preheated cell.

Fig. 11g-l show the SEM images of the cathodes, where Fig. 11g to i are the cathodes from the top, center, and bottom sections of the preheated cell, and Fig. 11j and k are the cathodes from the top and center sections of the control group cell. It can be seen that the secondary particles of the cathodes of the control group cell have slightly better integrity than the cathodes of the preheated cell, but the difference is not that evident compared to their anodes. Delamination was noticed on the NMC particles of both cells, and it was also observed that more primary particles are isolated from the secondary particles on the cathodes of preheated cell than the control group cell. A high magnification image of the delaminated particles is given in Fig. 11l. These physical damages can lead to the loss of lithium ions and formation of passive film on the fresh surfaces, as well as the loss of active materials due to the loss of electrical contact with the secondary particles and conductive fillers [28].

As a summary, durability tests have been carried out to investigate the side effects of multiple preheating at low temperature on a lithium-ion cell. It was found that the cell degraded faster in both power and energy if it operated in an extremely cold condition even with an appropriate external preheating measure taken. The SEM test further explained the causes of the degradation; on the anode side, graphite layers have exfoliated from the individual flakes, which will lead to the loss of active materials and lithium ions, as well as increased internal resistance. As for the cathode, delamination was noticed on some of the primary particles, and some of them were separated from the secondary particles, which will lead to the loss of active materials and lithium ions. No differences were observed among the electrodes that were taken from different locations of the preheated cell, indicating that the degradation is mainly because of the extremely low temperature and the preheating process, while the location of heater is not a dominating factor. The phase change of the electrolyte at low temperature could be the cause of the physical damage to the active materials. To improve the low temperature durability of the cells, coating could be used on the

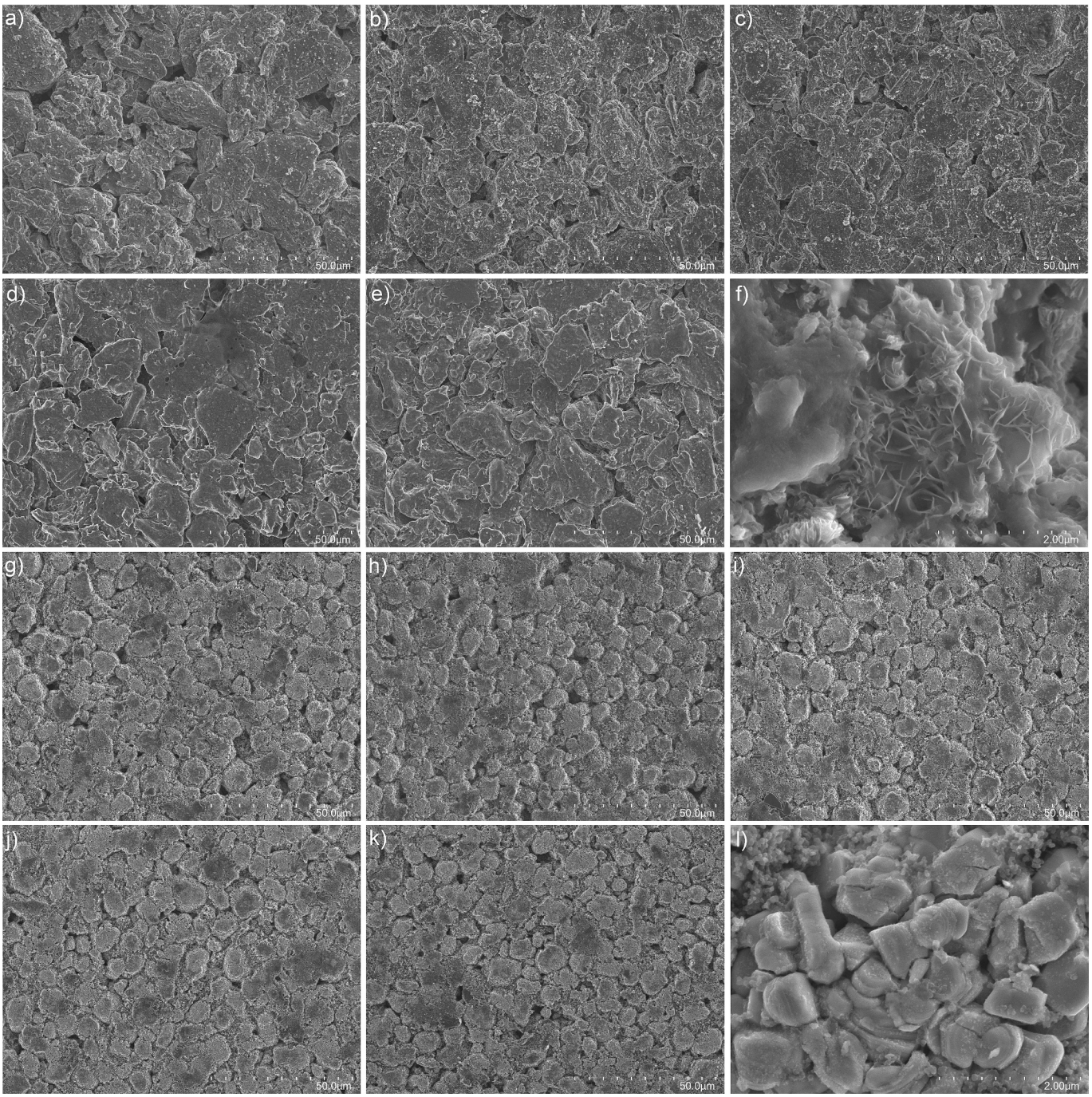

Fig. 11. SEM images of the anodes that were taken from the a) top, b) center, and c) bottom of the preheated cell, and d) top and e) center of the control group cell; e) the zoomed SEM image of the red square that shows the graphite exfoliation, and the SEM images of the cathodes that were taken from the g) top, h) center, and i) bottom of the preheated cell, and j) top and k) center of the control group cell; l) the zoomed SEM image of the delaminated NMC particles. (For interpretation of the references to colour in this figure legend, the reader is referred to the web version of this article.)

electrode particles to enhance their integrity [29] and low temperature electrolyte could also be used [30].

4. Conclusion

In this work, two external heating approaches, surface heating and tab heating, for cells at low temperature, were investigated for their performance on a pouch type cell. Both heating approaches were compared in terms of their heating time, hot spot temperature, and temperature uniformity. It was found that with proper insulation, at a similar heating power, both heating methods took similar time to bring the cell from −30 °C to 0 °C. However, the hot spot temperature of the cell heated through tabs was much higher than that of the cell heated through the surface, which restricted the cell from heating quicker than 10 min, at which the temperature of the positive tab has reached 70 °C. In comparison, when heated through the surface, it took less than 5 min for the cell to reach 0 °C at a heating power of 56 W, and the hottest spot on the cell was below 30 °C.

A thermal model was then developed and validated to help understand the limiting factors of the tab heating process. Four variables, tab size and thickness, thermal contact resistance between tabs and current collectors, as well as the current collector thickness, were adjusted in the

thermal model to investigate their effects on reducing the hot spot temperature and preheating time. Increasing the tab size and thickness are the two potential ways that can reduce the hot spot temperature. However, it was found that the OEM EV cells have much smaller tab area compared to the cell selected in this test, which is because the size and thickness of the tabs for a specific cell were designed based on the current flow instead of the heating performance. An inspection of the tabs inside battery modules further proved that tab heating is not suitable and ready for the cells due to the rough welding spots. Surface heating is a better option and more reliable preheating approach than the tab heating for the current EV pouch cells.

Durability and surface morphology tests were conducted on the surface heated cell and a control group cell that was cycled in ambient to study the effect of long-term preheating on cell's performance and durability. The cell that experienced continuous preheating cycles fades three times quicker than the cell cycled in ambient. Both voltage and incremental capacity curves indicates that the preheated cell experienced both capacity loss and internal resistance increase. Through SEM analysis, it was observed that the graphite layers were exfoliated from the anodes and some primary particles were isolated from the secondary particles on cathodes in the preheated cell, which leads to the loss of active materials and lithium ions, and resistance increase. In addition, it was noticed that the electrodes that close to the heater have very similar morphology as those from the center and the bottom of the cell, indicating that the temperature non-uniformity during the preheating stage may not pose non-uniform degradations between electrodes.

To sum up, due to the severely deteriorated performance and durability at low temperatures, maintaining the temperature of Li-ion batteries above a certain threshold during cold days through a battery thermal management system is critical. Tab heating could be a good approach to evenly preheat the cell only if modifications are made to the tabs and busbars of current pouch batteries to improve the heat transfer and thermal contact with the heater. Otherwise, surface heating or other effective means of preheating need to be designed and deployed on the pouch cells. For future works, research will be focused on developing preheating techniques that have minimal side effects on cells' performance and durability. In addition, preheating will be investigated on larger prismatic cells and cylindrical cells as they are widely used in the newly released EVs.

CRediT authorship contribution statement

Rui Zhao: Writing – original draft, Project administration, Investigation, Funding acquisition, Formal analysis, Conceptualization. **Vinayan Chittezhath:** Software, Data curation. **Dean D. MacNeil:** Writing – review & editing, Project administration, Funding acquisition.

Declaration of competing interest

The authors declare that they have no known competing financial interests or personal relationships that could have appeared to influence the work reported in this paper.

Acknowledgement

The authors would like to sincerely thank the funding support from the Advanced Clean Energy (ACE) Program from National Research Council of Canada. We also appreciate the help from Oltion Kodra in preparing the SEM images, as well as the discussion with Steven Recoskie and Giulio Torlone.

Data availability

Data will be made available on request.

References

[1] F. Degen, M. Winter, D. Bendig, J. Tubke, Energy consumption of current and future production of lithium-ion and post lithium-ion battery cells, Nat. Energy 8 (2023) 1284–1295.
[2] Global EV Outlook 2025, International Energy Agency. Global EV Outlook 2025 – Analysis – IEA, (Accessed 14 August 2025).
[3] Achieving a zero-emission future for light-duty vehicles, Environment and Climate Change Canada, https://www.canada.ca/content/dam/eccc/documents/pdf/cepa/achieving-zero-emission-future-light-duty-vehicles.pdf. (Accessed 14 August 2025).
[4] S. Zhang, K. Xu, T. Jow, The low temperature performance of Li-ion batteries, J. Power Sources 115 (2003) 137–140.
[5] Z. Guo, J. Zhu, J. Feng, S. Du, Direct *in situ* observation and explanation of lithium dendrite of commercial graphite electrodes, RSC Adv. 5 (2015) 69514.
[6] S. Vikram, S. Vashisht, D. Rakshit, M.P. Wan, Recent advancements and performance implications of hybrid battery thermal management systems for electric vehicles, J. Energy Storage 90 (2024) 111814.
[7] H. Luo, Y. Wang, Y. Feng, X. Fan, X. Han, P. Wang, Lithium-ion batteries under low-temperature environment: challenges and prospects, Materials 15 (2022) 8166.
[8] M. Storch, J. Fath, J. Sieg, D. Vrankovic, C. Krupp, B. Spier, R. Riedel, Temperature and lithium concentration gradient caused inhomogeneous plating in large-format lithium-ion cells, J. Energy Storage 41 (2021) 102887.
[9] A. Laforgue, X. Yuan, A. Platt, S. Brueckner, F. Perrin-Sarazin, M. Toupin, J. Y. Huot, A. Mokrini, Comparative investigation of the impact of fast charging at low temperature on commercial Li-ion cells, J. Power Sources 524 (2022) 231071.
[10] A. Khan, S. Yaqub, M. Ali, A.W. Ahmad, H. Nazir, H.A. Khalid, N. Iqbal, Z. Said, K. Sopian, A state-of-the-art review on heating and cooling of lithium-ion batteries for electric vehicles, J. Energy Storage 76 (2024) 109852.
[11] C.Y. Wang, G. Zhang, S. Ge, T. Xu, Y. Ji, X.G. Yang, Y. Leng, Lithium-ion battery structure that self-heats at low temperatures, Nature 529 (2016) 515–518.
[12] G. Zhang, S. Ge, T. Xu, X.G. Yang, H. Tian, C.Y. Wang, Rapid self-heating and internal temperature sensing of lithium-ion batteries at low temperatures, Electrochim. Acta 218 (2016) 149–155.
[13] H. Ge, J. Huang, J. Zhang, Z. Li, Temperature-adaptive alternating current preheating of lithium-ion batteries with lithium deposition prevention, J. Electrochem. Soc. 163 (2016) A290–A299.
[14] J. Zhu, Z. Sun, X. Wei, H. Dai, W. Gu, Experimental investigations of an AC pulse heating method for vehicular high power lithium-ion batteries at subzero temperatures, J. Power Sources 367 (2017) 145–157.
[15] S. Guo, R. Yang, W. Shen, Y. Liu, S. Guo, DC-AC hybrid rapid heating method for lithium-ion batteries at high state of charge operated from low temperatures, Energy 238 (2022) 121809.
[16] G. Cheng, Z. Wang, X. Wang, Y. He, All-climate thermal management structure for batteries based on expanded graphite/polymer composite phase change material with a high thermal and electrical conductivity, Appl. Energy 322 (2022) 119509.
[17] M. Klein, S. Tong, J.W. Park, The performance effects of edge-based heat transfer on lithium-ion pouch cells compared to face-based systems, SAE Technical Paper 01 (2014) 1866.
[18] I.A. Hunt, Y. Zhao, Y. Patel, G.J. Offer, Surface cooling causes accelerated degradation compared to tab cooling for lithium-ion pouch cells, J. Electrochem. Soc. 163 (2016) A1846–A1852.
[19] Y. Zhao, Y. Patel, T. Zhang, G.J. Offer, Modeling the effects of thermal gradients induced by tab and surface cooling on lithium ion cell performance, J. Electrochem. Soc. 165 (2018) A3169–A3178.
[20] S.H. Ham, D.S. Jang, M. Lee, Y. Jang, Y. Kim, Effective thermal management of pouch-type lithium-ion batteries using tab-cooling method involving highly conductive ceramics, Appl. Therm. Eng. 220 (2023) 119790.
[21] R. Zhao, J. Liu, J. Gu, The effects of electrode thickness on the electrochemical and thermal characteristics of lithium-ion battery, Appl. Energy 139 (2015) 220–229.
[22] P.M. McGuiggan, A. Chiche, J.J. Filliben, D.J. Yarusso, Peel of an adhesive tape from a temperature-gradient surface, Int. J. Adhes. Adhes. 28 (2008) 185–191.
[23] J. Liu, Q. Duan, K. Qi, Y. Liu, J. Sun, Z. Wang, Q. Wang, Capacity fading mechanisms and state of health prediction of commercial lithium-ion battery in total lifespan, J. Energy Storage 46 (2022) 103910.
[24] W. Diao, J. Kim, M.H. Azarian, M. Pecht, Degradation modes and mechanisms analysis of lithium-ion batteries with knee points, Electrochim. Acta 431 (2022) 14143.
[25] M. Bettge, Y. Li, K. Gallagher, Y. Zhu, Q. Wu, W. Lu, I. Bloom, D.P. Abraham, Voltage fade of layered oxides: Its measurement and impact on energy density, J. Electrochem. Soc. 160 (2013) A2046–A2055.
[26] L. Spitthoff, P.J.S. Vie, M.S. Wahl, J. Wind, O.S. Burheim, Incremental capacity analysis (dQ/dV) as a tool for analysing the effect of ambient temperature and mechanical clamping on degradation, J. Electroanal. Chem. 944 (2023) 117627.
[27] S. Barcellona, S. Colnago, G. Dotelli, S. Latorrata, L. Piegari, Aging effect the variation of Li-ion battery resistance as function of temperature and state of charge, J. Energy Storage 50 (2022) 104658.
[28] P.M. Attia, et al., Review – "Knees" in lithium-ion battery aging trajectories, J. Electrochem. Soc. 169 (2022) 060517.
[29] Z. Zhu, F. Cai, J. Yu, Improvement of electrochemical performance for AlF_3-coated $Li_{1.3}Mn_{4/6}Ni_{1/6}Co_{1/6}O_{2.4}$ cathode materials for Li-ion batteries, Ionics 22 (2016) 1353–1359.
[30] S. Yun, X. Liang, J. Xi, L. Liao, S. Cui, L. Chen, S. Li, Q. Hu, Electrolytes for high-safety lithium-ion batteries at low temperature: A review, Polymers 16 (2024) 2661.